47th AIAA/ASME/ASCE/AHS/ASC Structures, Structural Dynamics, and Materials Confere
1 - 4 May 2006, Newport, Rhode Island

AIAA 2006-1620

A System for Aerothermodynamic, Servo, Thermal, Elastic, Propulsive Coupled Analysis (ASTEP)

Kevin M. Roughen[*], Myles L. Baker[†], and Guclu Seber[‡]
M4 Engineering, Signal Hill, California, 90755

and

Trent M. Taylor[§]
University of Missouri-Rolla, Rolla, Missouri, 65409

The ASTEP System is a multi-disciplinary software tool for coupled analysis of high speed airbreathing flight vehicles. Design of a capable hypersonic vehicle requires consideration not only of the traditional aerospace engineering disciplines, but also of the interactions among them. Application of state of the art simulations of multiple disciplines with a coupled approach has traditionally led to a choice between significant decreases in fidelity and prohibitive increases in computational cost. The ASTEP System applies an existing efficient aerodynamics solver to significantly reduce computational cost. This enables a multi-disciplinary approach that can be applied to analyze the interactions along a complete trajectory with a relatively high level of fidelity. This paper describes the capabilities of Build 1 of the ASTEP System including modules addressing geometry, trajectory, trim, aerodynamics, propulsion, thermal, and structural disciplines.

I. Introduction

As aerospace vehicles progress into the hypersonic regime, new challenges face the design engineer. Successful design of this type of vehicle clearly requires the capability to analyze high-speed aerodynamics, propulsion systems involving supersonic mixing and combustion, high-temperature thermal protection systems, airframes under extreme loads, and control systems capable of stabilizing the vehicle in a broad range of flight conditions. What is less readily apparent is that in the hypersonic regime, these analyses are tightly coupled and the interactions among them cannot be neglected. Small changes in shape due to pressure and thermal loading can significantly change the aerodynamics, which in turn changes the efficiency of the propulsion system and the aerodynamic and thermal loads. While traditional engineering approaches often attempt to separate analyses into disciplines, current vehicles demand that analyses be performed in a multi-disciplinary manner. For the next generation of vehicles, failure to achieve an early and accurate representation of the physics within and among disciplines can easily result in failure of the program.

In a process with efficient integration of disciplinary analyses, the time spent within the disciplinary analyses becomes the primary cost consideration. In fact, it is often the case that one discipline significantly affects the time required for the entire process. The viability of a system for aerothermodynamic, servo, thermal, elastic, propulsive (ASTEP) couple analysis is highly dependent on the selection of an accurate and efficient aerothermodynamic solver. Computational Fluid Dynamic (CFD) methods required for accurately representing the relevant physics have traditionally been very time consuming. Recent methods providing more efficient solutions enable a viable CFD based ASTEP process. In the ASTEP system, modern CFD methods will allow for a tool that is both highly accurate and computationally inexpensive. Taking full advantage of the approaches used in developing the IHAT multidisciplinary analysis/optimization toolkit, this core capability of aerothermal analysis is integrated into an automated ASTEP software product. This product accurately represents aerothermodynamic pressure and temperature, propulsive force and heat, ablation thickness, and structural deflection. The interactions of these effects

[*] Senior Engineer, 2161 Gundry Avenue, Member AIAA.
[†] Chief Engineer, 2161 Gundry Avenue, Associate Fellow AIAA.
[‡] Senior Engineer, 2161 Gundry Avenue, Member AIAA.
[§] Graduate Research Assistant, 1870 Miner Circle, Student Member AIAA

is represented in an algorithm that iterates until a solution is reached which represents the relevant physics within and among the disciplines.

II. Geometry Module

The main purpose of the geometry module is to transfer shape changes due to elastic, thermoelastic, and control deflections to the CFD model. A point-cloud based morphing algorithm is applied. The morphing algorithm has been used quite successfully for updating aerodynamic models due to design variable changes, and has been implemented as an option in a variant of the CFL3Dv6 code.

The morphing algorithm used in the ASTEP System is based on a background mesh approach. Starting with the baseline finite element model nodes, a background mesh is generated that covers the "near field" volume around the vehicle. Each node in the baseline CFD model is then mapped to a given position in a given element in the background mesh. When the positions of finite element nodes are updated, the background mesh moves to accommodate the new shape, and all embedded CFD points simply follow along. This approach is very fast and robust to many types of shape changes. Since it is a point-cloud approach, it is equally applicable to structured and unstructured grids. The process is shown schematically in the figure below.

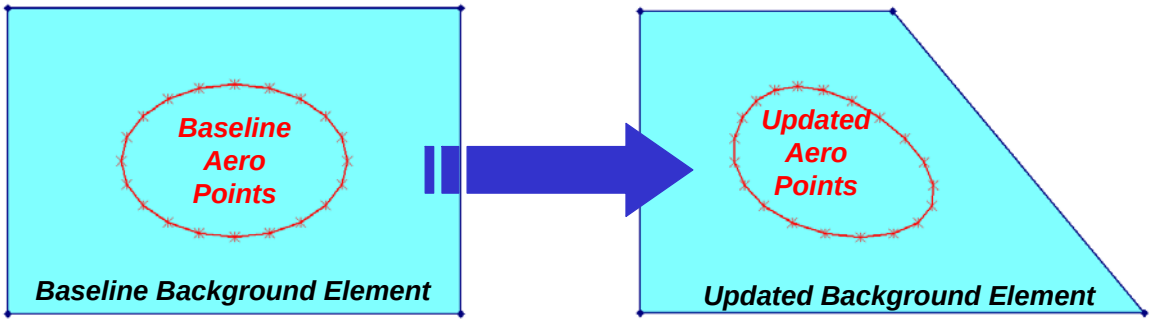

Figure 1. 2-D illustration of the Morphing algorithm, which allows quick and robust updates to make CFD model conform to updated geometry.

III. Trajectory Module

The equations of motion of the vehicle include equations for position (altitude and downrange coordinates), speed, flight path angle, and vehicle mass. For the vehicle mass equation, the fuel mass flow rate is calculated directly by the propulsion module. The integration algorithm used in the current implementation is Euler's method. This method was chosen for its simplicity and facilitated demonstration in Build 1.

IV. Trim Module

The purpose of the trim module is to guide the vehicle along the target trajectory. In order to make it feasible to simulate a complete trajectory using CFD simulation data, this is performed using a feedback control approach, rather than by explicitly iterating each time step to convergence. This approach introduces some approximation errors if the time steps are large, but provides great advantages in efficiency. An option is available to allow subiterations to improve convergence if the errors exceed a user-specified tolerance.

The overall approach of this algorithm is to take advantage of the fact that the vehicle flying along a trajectory is essentially a dynamic system, and keeping the vehicle on the desired trajectory can be viewed as a simple regulator problem. In this implementation, the target trajectory is checked at each time step, and the vehicles actual position is compared to the target trajectory. This makes it possible to calculate a speed error, a flight path angle error, and a pitching moment error. The settings of the throttle, the angle of attack, and the control surfaces (fins/elevators) are then set in order to reduce these errors as rapidly as possible. It must be emphasized that this capability offers a trade-off between accuracy and efficiency. Without subiterations, the vehicle may not satisfy the moment equilibrium equations at every time step. The impact of this approximation must be evaluated by the user, and a determination must be made whether subiterations are required.

V. Aero-Propulsion Integration

A. Aerodynamic Modeling

A structured multi-block CFD code is used for the aerodynamic modeling in ASTEP. The code is obtained as source code and then configured to the users' system needs and then compiled. This directly compiled source code runs much more quickly than most other package CFD codes while still maintaining an accurate result.

The code was originally tested using both caloricly and thermally perfect models and a small but unsubstantial increase in run time was seen for thermally perfect; however, the thermally perfect model was still chosen. This is because of the high temperatures in ramjet/scramjet flow which are not conducive for accurate results for constant gamma flow. The code makes use of thermodynamic databases have one, two, or three temperature intervals for the species curve fits. Time trials were also conducted for these intervals, and for the cases considered, the increase in run time for the three-interval curve fits was very small. The large temperature range for which the thermodynamic values are accurate, help to ensure convergence in flow-fields with large gradients; which have extreme transient behavior before convergence.

Depending on whether viscous and heat transfer effects are of interest in the simulation, Euler or full viscous Navier-Stokes simulations can be conducted. If the full Navier-Stokes is chosen to be run, a variety of wall conditions can be utilized. A few on the list are: adiabatic wall, isothermal wall, specified temperature distribution wall, and also a specified wall thickness and thermal conductivity.

An example vehicle is shown below. Notice the abrupt change in the contours at the exit of the combustor. This is from the aero/propulsion integration. The CFD solver has the ability to split the flow-field into different 'regions.' Each region can be individually set so that it has its own solver characteristics and can either be active or not for each execution. The CFD solver is used to solve the whole external flow and through the combustor so that accurate predictions of the aero-elastic and heating effects, as well as vehicle forces, can be found; however, the CFD solver is not used to model the fuel mixing and combustion for this package. To do so would drastically increase the run time. The part of the flow-field up to an isolator/combustor entrance is set as a region and only that region is initially solved. The CFD solver then post processes on that entrance plane and then 1-D conserved flux flow values can then be found. These values are then passed to RJPA which provides a good model of the mixing and reaction in the combustor and also accounts for any increase in heat transfer in the combustor. RJPA then outputs 1-D combustor exit conditions. The rest of the regions in the flow-field are then solved. It solves through the combustor and at the exit plane, the 1-D values from RJPA are set as an inflow boundary condition, then a CFD solution is obtained through the nozzle. The CFD solver also has the ability to make a mixture species to use for the solution process. An air species is used for the inflow to the vehicle and a combustion product species is used at the combustor exit, both of which are modeled as thermally perfect (gamma varies with temperature). The combustion species is made from combining the curve fits from the individual product species and varies with equivalence ratio. This is done to decrease the run time since only two species are used to model the air and all the combustion products and to still have accurate thermodynamic properties at the combustor exit and have mixing of the two species in the nozzle plume.

Figure 2. Representative CFD solution. Symmetry plane of 3-D model shown.

B. Combustor Modeling

While the flow of air through the propulsion flowpath is included in the CFD simulation, the actual combustion and propulsion calculations are performed using a control volume analysis based on the Ramjet Propulsion Analysis (RJPA) code from Johns-Hopkins University Applied Physics Laboratory. This software was also used in the IHAT system as one of the propulsion analysis options. In this analysis, the stream-thrust averaged properties at the inlet throat are calculated using the CFD simulation results. These quantities include the total mass, momentum, and energy going into the inlet throat. These are used to develop an input file for RJPA. Along with the inlet conditions, RJPA requires an additional input file defining the amount of fuel being supplied. Finally, a third file is required that defines basic combustor parameters such as inlet area, exit area, wall surface area, friction factors, combustion efficiency, etc.

Based on these inputs, RJPA performs a chemical equilibrium analysis to determine the combustion products. This includes a complete chemical species description, as well as a complete thermodynamic description including molecular weight, enthalpy of formation, ratio of specific heats, and average temperature, velocity, and pressure at the combustor exit plane. The temperature, velocity, and pressure at the combustor exit plane are then applied as a boundary condition in the CFD simulation to simulate the exhaust plume.

C. Combustor Inflow

A special method must be used in order to post process the combustor inflow to get the 1-D stream thrust averaged flow values. The first region is solved up to the combustor entrance. The inlet exit plane is then set as an outflow boundary and a profile is written of the flow and the CFD solver then post processes that plane. This 'profile' contains all the flow information across the plane so the 3-D aspect of the flow is preserved. A script was written to search for a user-defined text string (which is of the block and face of the combustor entrance plane) in the post processor results. The script then uses the CFD results to find the conserved flux flow parameters to pass to RJPA. When the rest of the regions are run, the profile that was written out from the first run is then used as the inflow plane for the combustor.

D. Combustor Outflow

The CFD solver solves through the combustor as a 3-D duct. When it reaches the combustor exit plane, and extrapolated outflow boundary condition is used at the exiting block face. The next block face (nozzle entrance plane) is point-to-point continuous with the outflow plane from the combustor. The CFD solver is able to specify two different boundary types for the same co-incident plane that is the boundary between two different blocks. The nozzle entrance plane uses a FIXED boundary condition which contains the 1-D flow properties found from RJPA. It only requires density, velocity, and temperature to define the boundary condition (as well as the species type). The thermodynamic database will be updated to contain a combustion product species that is dependent on the equivalence ratio of the combustor, and this species is set as 100% of the mass fraction at this plane. From this 'inflow' plane, the combustion product species has frozen composition (still with temperature variable gamma). It then flows through the nozzle and mixes with the air species in the plume.

E. Overall Vehicle Forces and Moments

Overall vehicle forces and moments are calculated by integrating the pressures on the external surfaces of the vehicle, and applying a correction for the thrust generated in the combustor itself. This correction is based on the stream thrust of the fluid entering the inlet throat, and the stream thrust of the fluid exiting the combustor exit. The current software implementation assumes that all flow in the combustor is in the axial (x) direction. While this is accurate for the current waverider model, an enhancement to address the vertical component of flow into and out of the combustor may be required for other configurations.

The implementation of this procedure is as follows. The post processor prints a global summary at the end of the results. This contains the total wall forces from pressure and shear, as well as the moment created from these wall forces. The CFD solver does solve through the combustor, but RJPA is used to model the reaction in the combustor. Therefore, the effect on the global wall force from the combustor that is found using the CFD solver is removed from the global result. The change in stream thrust through the combustor is used to find the influence of the combustor on the vehicle forces. This is calculated from the previously post processed combustor entrance plane, and another user defined text string, which defines the nozzle entrance plane, is used to search for another set of post processed results to calculate the exiting stream thrust. So, the overall vehicle forces and moments are found from the integrated pressures and shear on all vehicle wetted surfaces, except the combustor, whose influence is accounted for by the change in stream thrust.

VI. Thermal Module

A. Introduction

The ASTEP Thermal Module is constructed around the CFD aeroheating solver and a 1-D Ablation and Conduction (ODAC) code developed under this project. Taking this approach in the Build 1 effort alleviated the schedule impact associated with integration of existing off-the-shelf codes.

B. Heat Flux Mapping

The thermal analysis within ASTEP is performed at the centroid of each element of the structural model. In other words, the thermal model is identical to the structural model. Software has been developed that reads the structural and aerothermodynamic models and maps the aerothermodynamic grid onto each structural element in a user specified list. This allows the user to specify only structural elements that are in contact with the flow. In order to save computational time, this mapping information is computed once and saved. For each iteration, a program is executed that takes the heat flux data from the CFD output file and associates it with the appropriate thermal elements. Variables are present within the system to allow for scaling of length and heat data if necessary to accommodate models built in different unit systems.

C. Conduction Analysis

An in-house routine for 1-D (through the thickness) heat conduction has been implemented in Build 1. This software solves the classic conduction equation $\delta T/\delta t = \alpha\ \delta^2 T/\delta x^2$. The solution is performed in the implicit form and takes advantage of the efficiency possible from tri-diagonal matrices. The routine for 1-D conduction has been validated against a closed form solution for an infinite slab. Excellent correlation is observed as shown in the figures below.

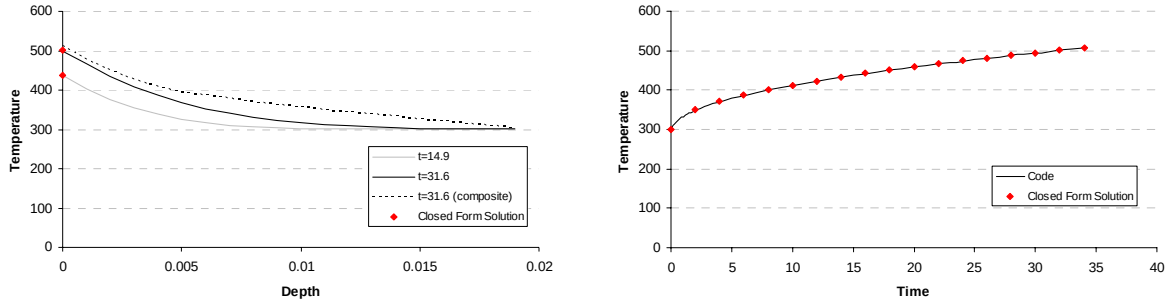

Figure 3. Correlation of ODAC to closed form conduction solution.

D. Ablation Model

In the current effort, a simplified approach has been implemented to model the q* effect of ablation. The heat of ablation is characterized the specific heat capacity of a material as a function of temperature. An increase in the specific heat capacity is specified between the ablation temperature and a tolerance above it. This data is modified so that the additional heat required to raise the temperature above this tolerance is equal to q*. It is noted that this approach cannot represent an ablative material going through the irreversible process of cooling back through its ablation temperature. This approach demonstrates the feasibility of handling ablation within this system.

VII. Structural Module

A. Pressure Loading

The aerodynamic loading is obtained through mapping the CFD pressure onto the structural model. This involves an algorithm that obtains the n nearest structural nodes to each CFD surface patch. Once this set of nodes is determined, a transformation matrix is computed that distributes the pressure load to the surrounding nodes while conserving total force and moment. This approach has shown excellent results both in terms of conservation of forces and moments, and in terms of qualitative force distribution. A validation result for this technique (shown on a subsonic wing) is shown below.

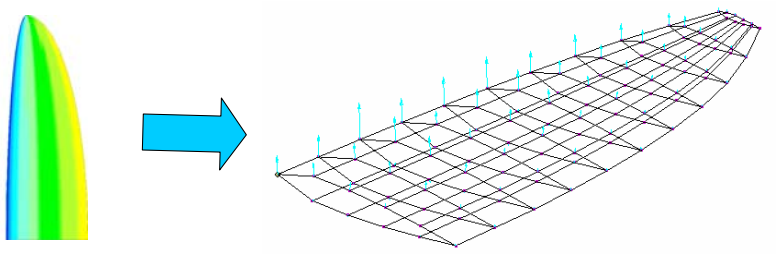

Figure 4. Schematic of Force Mapping Algorithm and Result.

B. Thermal Loading

The thermal loading is accomplished using the thermal loading capability within NASTRAN. The thermal and structural models are coincident, so once the heat flux data is mapped from the aerodynamic model within the Thermal Module, application of the temperature distribution to the structural model requires no additional transformation.

C. Inertia Loading

In order to have a balanced load condition for structural analysis, inertia loads must be applied that are consistent with the applied pressure loading. This is addressed in ASTEP through a utility that calculates inertia properties based on the mass and force data represented in the FEM. Though this capability is available in MSC/NASTRAN, this external utility provides the user of the ASTEP system flexibility to use other solvers. This routine outputs the residual force and moment as a check, and these residual loads have been determined to be very small for example problems.

VIII. Waverider Example Vehicle

The primary example problem for the Build 1 demonstration of the ASTEP System is a generic waverider vehicle, which is shown in schematic side-view in Figure 5.

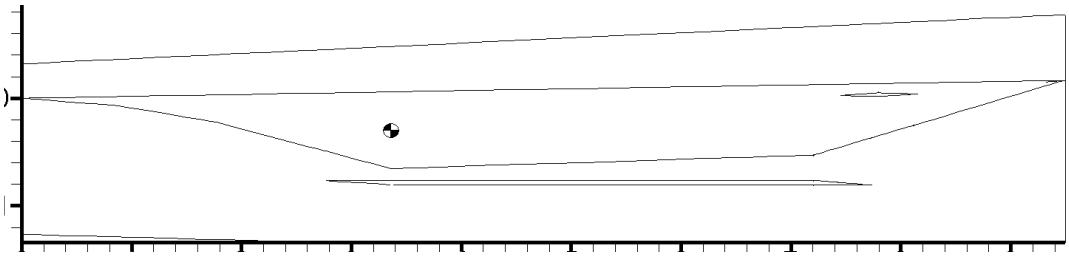

Figure 5. Example Vehicle Showing CG Location.

A. Aerodynamic Modeling

The 3-D grid used for the waverider example vehicle was generated using Gridgen. Figure 6 shows a sampling of the grid. The first shows the outline of the different blocks which compose the vehicle so that more detail can be seen of the vehicle and accompanying wing. The next shows the grid lines for the vehicle. Care was taken to keep the grid as economical as possible, reducing the number of grid points as much as possible without degrading accuracy.

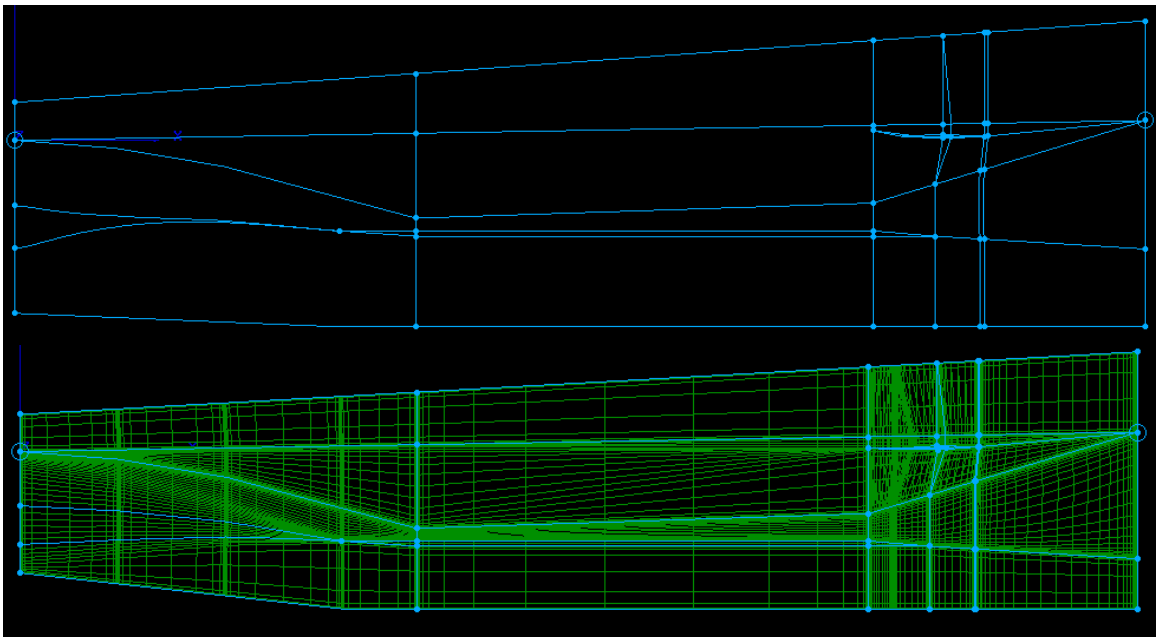

Figure 6. Example Vehicle Aerothermodynamic grid.

This figure below shows the vehicle surfaces created in Gridgen with the surface pressures displayed as a fringe. The wing can be seen to be attached to at the root to the vehicle in a diamond shape and is swept back and blend to a plate at the tip.

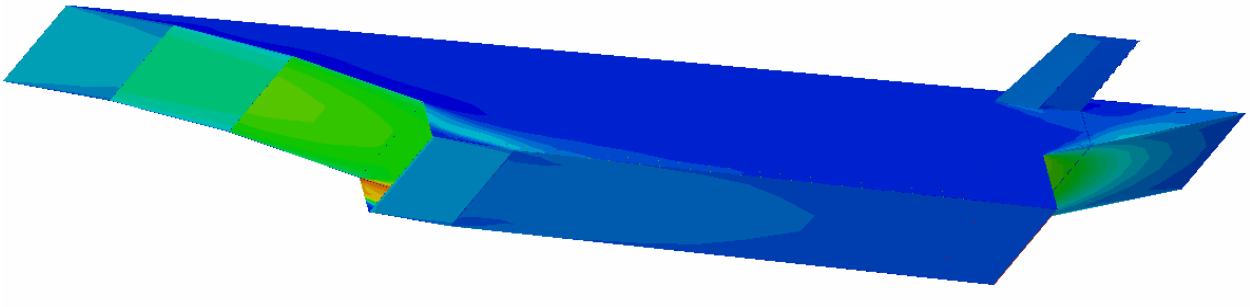

Figure 7. Representative pressure results on the waverider vehicle.

Figure 8 shows contours along the vehicle centerline, and Figure 7 shows the pressure contours on the vehicle. The pressure contours above show the 3-D relieving in the inlet and the shocks generated from the start of the cowl can be seen both inside and outside the combustor. The pressure can also be seen on the wing and filling the base of the nozzle. The contours below show the three-break inlet and the reflecting shocks going through the combustor. The discontinuity can also be seen at the combustor exit where the RJPA conditions are applied and the expansion in the plume.

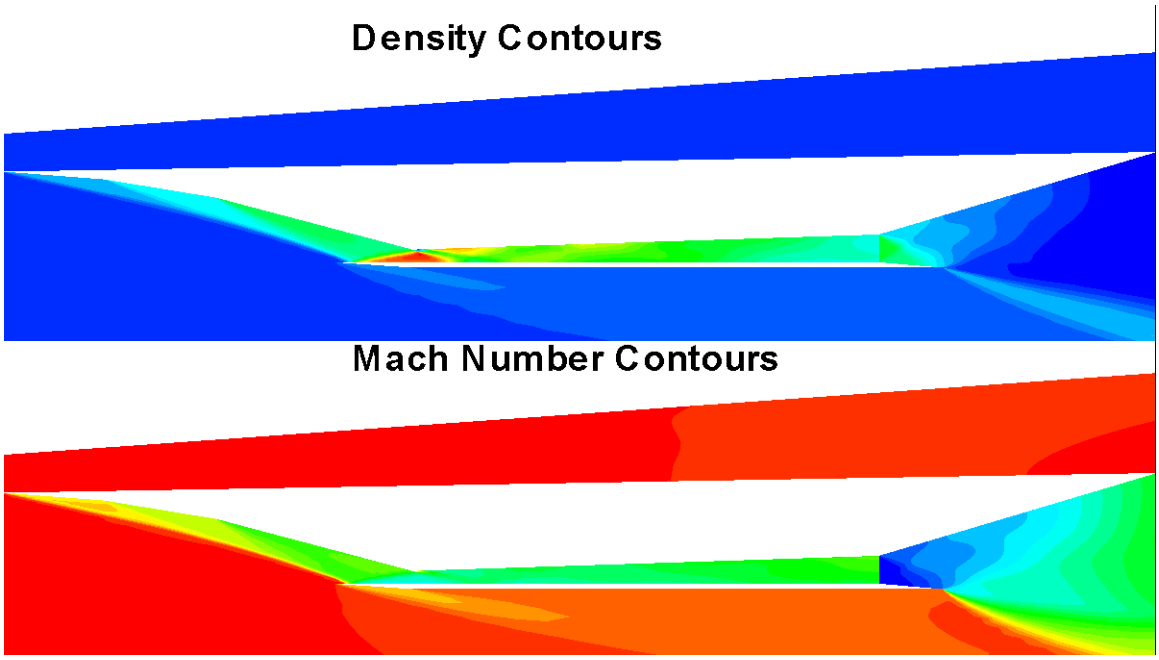

Figure 8. Example CFD Solutions (results on symmetry plane shown).

Some quantitative results from the integrated aero-propulsive model are shown in Figures 9 through 11. These charts are the results of running the ASTEP process through the Geometry and Aerodynamics/Propulsion Modules, and calculating the total resultant force on the vehicle. These forces were then normalized to give axial, normal, and pitching moment coefficients. In order to validate the key portions of the model (aerodynamics, propulsion, and trim), three separate sets of analyses were performed. The first is a throttle sweep, where the equivalence ratio is varied between 0.0 and 1.0. All analyses were performed at the same Mach number. These analyses were performed at angle of attack and fin deflection angle of zero degrees. The results are shown in Figure 9. The most obvious trend is that increasing fuel flow results in a more negative (less drag, more thrust) axial force coefficient. Another interesting trend that has a significant impact on the controllability of the vehicle is the large nose-down pitching moment that is caused by increasing throttle setting. This is due to the increased pressure on the free-expansion surface of the nozzle, which results in a net up-force on the aft portion of the vehicle. There is a significant, but weaker effect on the normal force coefficient.

Figure 10 shows the effect of varying the angle of attack, with fin deflection held constant at 0 degrees, and equivalence ratio held constant at 0.25. As expected, the dominant trend is increasing lift with angle of attack, as the reference point is very close to the aerodynamic center. There is a relatively weak influence of angle of attack on the axial force coefficient.

Figure 11 shows the isolated effect of changing the fin deflection. This was performed by using the mesh morphing capabilities of the Geometry module to update the CFD grid for each run. Increasing the fin deflection (sign convention nose up) results in a slight increase in vehicle lift, and a relatively large nose-down pitching moment.

These results demonstrate the robustness of the integrated aero-propulsion analysis, and provide the confidence required to implement the full trajectory simulation.

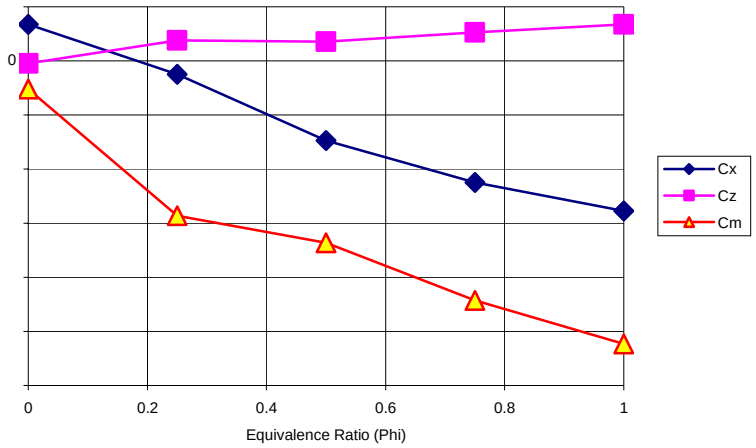

Figure 9. Variation in vehicle force coefficients with variations in throttle setting.

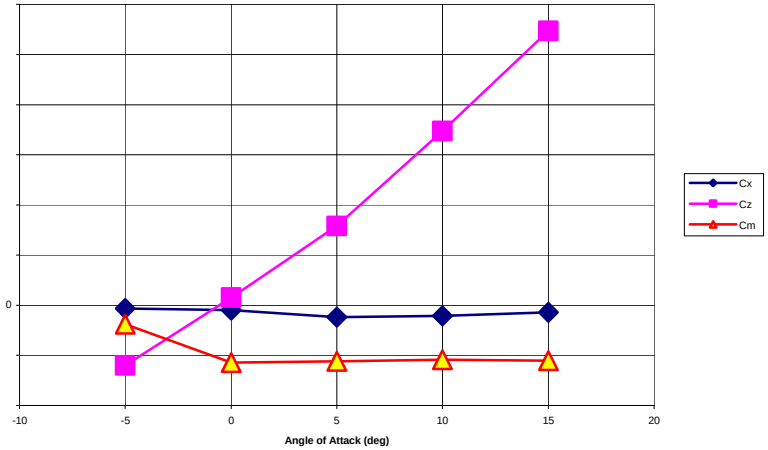

Figure 10. Variation in vehicle force coefficients with variations in angle of attack.

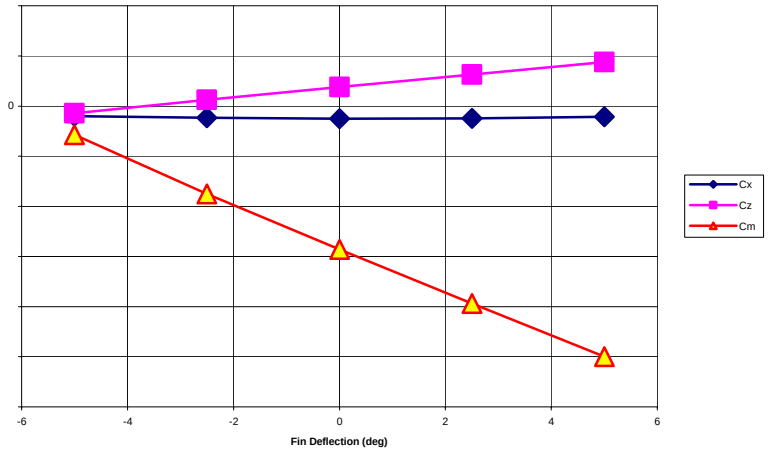

Figure 11. Variation in vehicle force coefficients with variations in fin deflection.

B. Structural Modeling

The definition of the structure of the vehicle is defined to the ASTEP system in the form of a NASTRAN Finite Element Model. The waverider example vehicle is represented with a shell element model representing the skins, bulkheads, and fins of the waverider structure. The model has 1785 nodes and 1820 elements and is shown in the figure below.

The material properties for this vehicle have been chosen to be representative of high speed vehicle. The properties are modeled to be representative of iso-grid structure to get an appropriate relationship between membrane and bending stiffness. The model was validated by performing a modal analysis. The first flexible mode shape is shown below. The mode shape exhibits coupled body and fin bending.

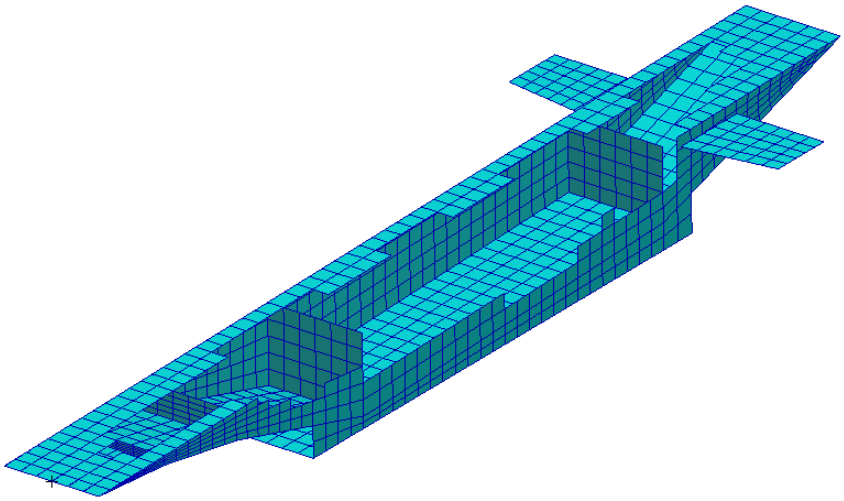

Figure 12. Structural Model for Waverider Example Vehicle.

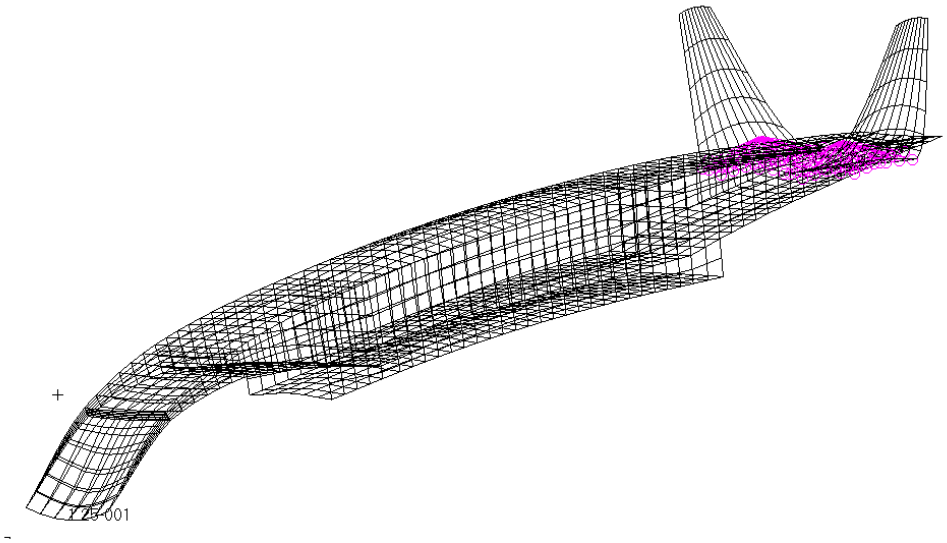

Figure 13. Structural Mode Shape for Waverider Example Vehicle.

C. Thermal Modeling

The thermal model for the example vehicle is modeled using a uniform property distribution. The thermal properties are for a two layer structure of ablative thermal protection above metallic structure. The ablative material is modeled to be representative of MCC-1.

IX. Aeroelastic Result

In order to provide intuitive aeroelastic behavior, a rotational spring was added at the root of the fin at 10% cord. This allows the fin to wash-out (unload) when the vehicle is at angle of attack. This behavior is seen in figures 8.3 (pressure profile) and 8.12 (structural deflection and FEM load vectors). These figures also show aeroelastic behavior at the lower combustor exit. In that region, the structure is soft and the pressure is high, leading to large displacement.

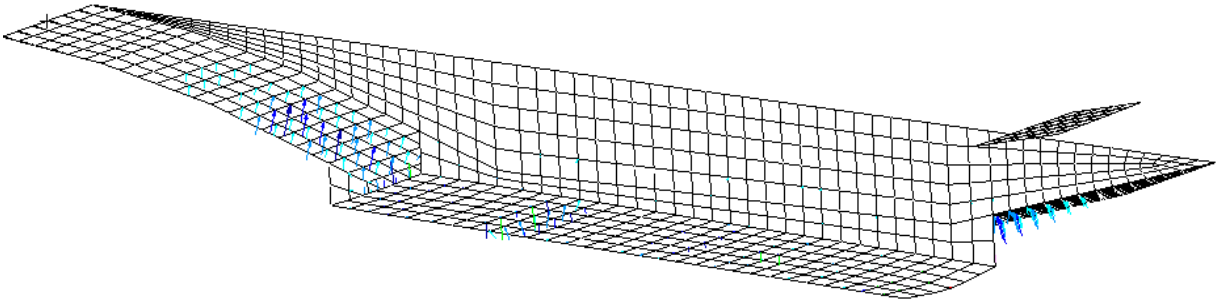

Figure 14. Structural Model Showing Mapped Aerodynamic Forces and Magnified Deflections for Waverider Example Vehicle.

X. Aerothermoelastic Result

Aerothermoelastic analysis has been performed for the waverider vehicle following the data path from the Aerothermodynamics Module to the Thermal Module. The condition run for demonstration is an engine-on condition that demonstrates significant heat flux on the vehicle surface aft of the combustor. This effect is well characterized in the CFD heat flux data, and can be clearly observed in the backface temperature data output from the thermal module.

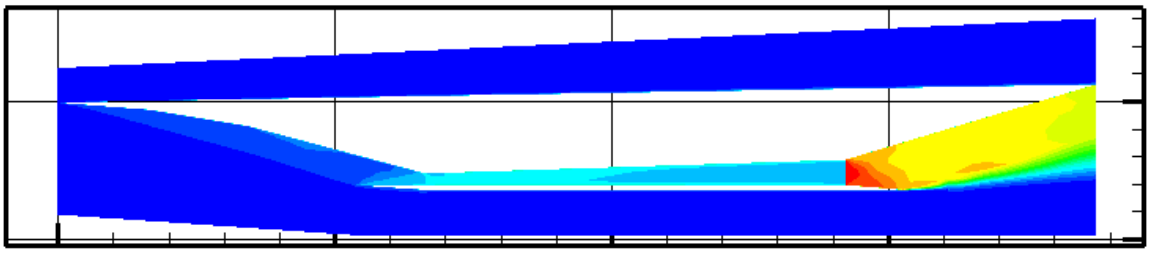

Figure 15. Centerline Temperature.

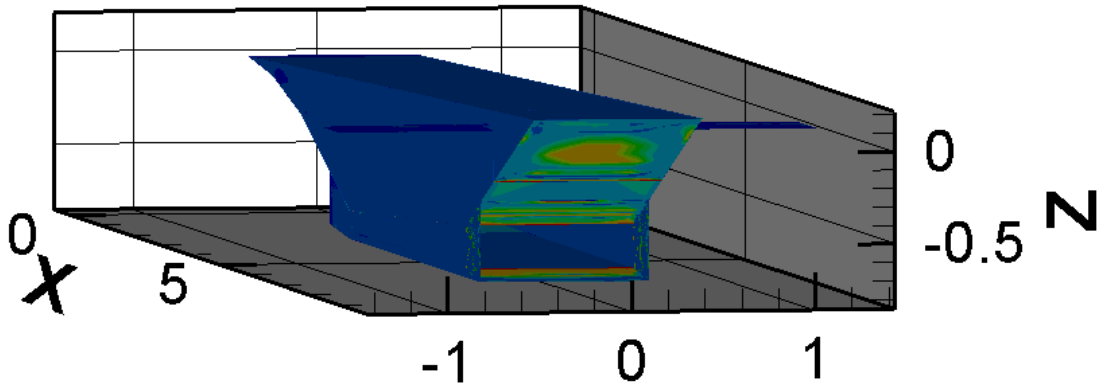

Figure 16. Heat Flux Distribution.

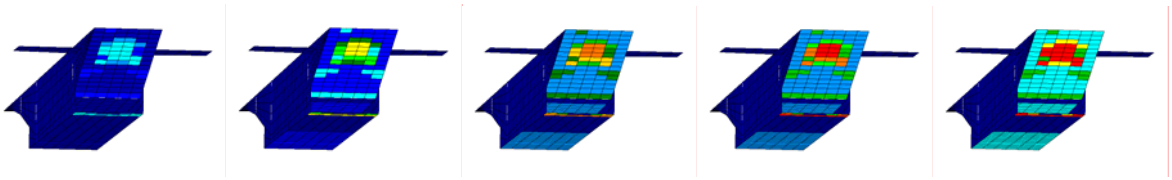

Figure 17. ODAC Back-face Temperature Results for Time=100-500 sec.

XI. Full Trajectory Simulation

A simulation of the generic waverider vehicle across a representative flight trajectory is shown in Figure 18. In this Figure, the target trajectory is described in terms of waypoints (pink squares). These waypoints are entered in time, altitude, range triples, and define the vehicle flight path and velocity profile. The ASTEP system was used to simulate the ASTEP trajectory (blue curve). As is clear from the Figure, the as-flown trajectory is a good approximation of (but not an exact match to) the target trajectory. The initial flight path angle of the vehicle was specified intentionally to be different from the initial flight path angle of the target trajectory. This results in the early deviation between the simulated and target trajectories, but shows that the simulation can recover from significant disturbances. Changing the gains in the feedback loops can be used to improve the fit between the target and actual trajectories.

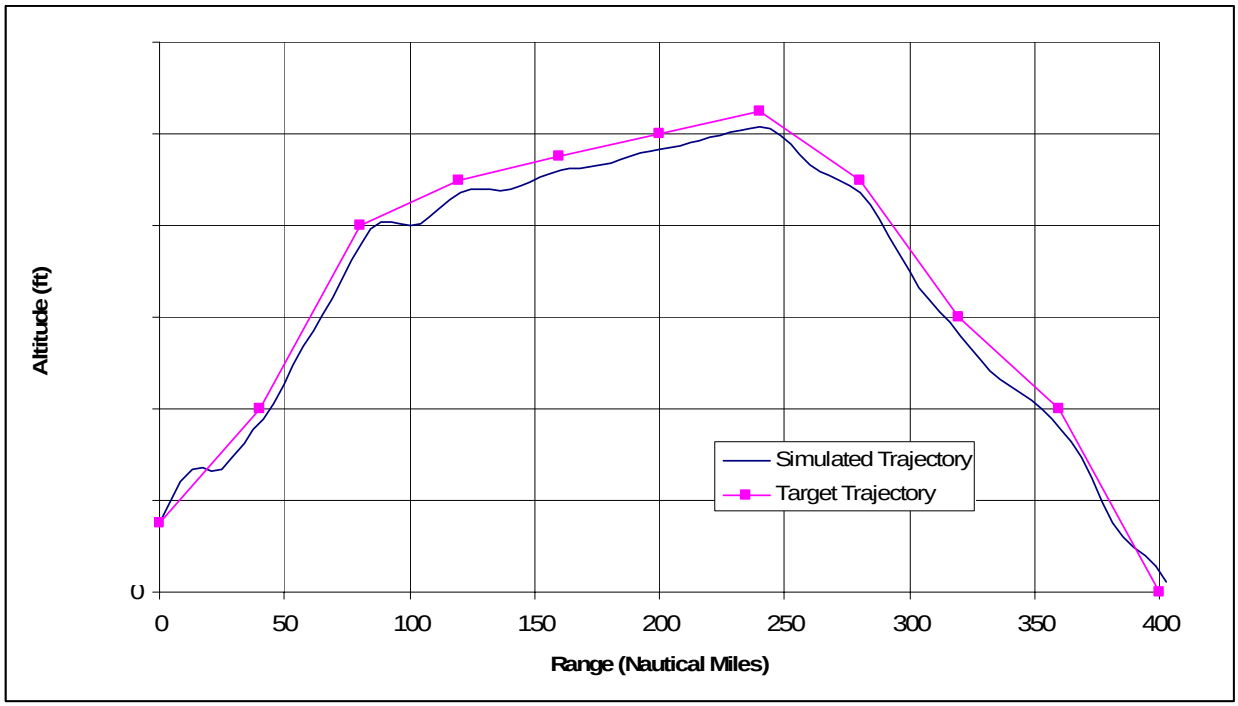

Figure 18 – Comparison of Target Trajectory (pink, input by user) and Actual Vehicle Trajectory (blue, calculated by code).

Acknowledgments

Funding for the development of the ASTEP System is provided by the Air Force Office of Scientific Research. The authors also wish to acknowledge the contributions of the rest of the ASTEP System team, without whose tireless efforts this work would not be possible.

References

1. Baker, M.L., Munson, M.J., Hoppus, G.W., and Alston, K.Y., "Integrated Hypersonic Aeromechanics Tool (IHAT), Build 4", presented at the 42nd AIAA Aerospace Sciences Meeting and Exhibit, Reno, Nevada, January 2004.

2. Baker, M.L., Munson, M.J., and Alston, K.Y., "Integrated Hypersonic Aeromechanics Tool (IHAT)", presented at the 9th AIAA/ISSMO Symposium on Multidisciplinary Analysis and Optimization, Atlanta, GA, September 2002.

3. *MSC.Nastran Linear Static Analysis User's Guide*, MSC Software, 2003.

4. Pandolfini, P.P. and Friedman, A.., *Instructurions for Using Ramjet Performance Analysis (RJPA)*, Johns Hopkins University Applied Physics Laboratory, JHU/APL AL-92-P175.

5. Bisplinghoff, R. L., Holt, A., and Halfman, R.L., *Aeroelasticity*, Dover Publications, Inc., New York, 1996.

6. Mills, A.F., *Basic Heat and Mass Transfer*, Richard D. Irwin, Inc., Massachusetts, 1995.

7. Thornton, E. A., *Thermal Structures for Aerospace Applications*, AIAA Education Series, AIAA, Virginia, 1996.

8. Hankey, W.L., *Re-Entry Aerodynamics*, AIAA Education Series, AIAA, Washington, DC, 1988.

9. Bertin, J.J., *Hypersonic Aerothermodynamics*, AIAA Education Series, AIAA, Washington, DC, 1994.

10. Heiser, W. H., Pratt., D. T. , Daley, D. H., Mehta, U. B. , *Hypersonic Airbreathing Propulsion*, AIAA Education Series, AIAA, Washington, DC, 1994

11. Le, A., Gray, K., and Baker, M.L., "Integrated Hypersonic Aeromechanics Tool Aerodynamics Module", presented at the 42nd AIAA Aerospace Sciences Meeting and Exhibit, Reno, Nevada, AIAA-2004-0215, January 2004.

12. Loundagin, J.A., Rice, T., and Moore, J.B., "Integrated Hypersonic Aeromechanics Tool Propulsion Module", presented at the 42nd AIAA Aerospace Sciences Meeting and Exhibit, Reno, Nevada, AIAA-2004-0858, January 2004.

13. Morris, R.J., Burnes, R.R., and Caulfield, J., "Integrated Hypersonic Aeromechanics Tool Thermal Module", presented at the 42nd AIAA Aerospace Sciences Meeting and Exhibit, Reno, Nevada, AIAA-2004-0489, January 2004.

14. Porter, C.S., Baker, M.L., Alonge, F.A., Sutton, M., and Munson, M.J., "Integrated Hypersonic Aeromechanics Tool Structural Module", presented at the 12th AIAA International Space Planes and Hypersonic Systems and Technologies, Norfolk, VA, AIAA-2003-7012, December 2003.